

# **Resonant Excitons in Strontium Titanate**

**Name: Tan Chian Wen Melvin**

**Matriculation Number: A0111064Y**

**Supervisor:**

**Assistant Professor Andrivo Rusydi**

**National University of Singapore**

**A thesis submitted to the Faculty of Science  
as a partial fulfilment of the Bachelors of  
Science (Hons.) in Physics**

**2017**

## **Acknowledgements**

I would like to express my greatest gratitude to Professor Andrivo Rusydi for his patience and guidance throughout the project. I would also like to thank Dr Pranjali for his help and answering my queries. Last but not least, I would like to thank my family and friends who have encouraged and supported me through the project.

# Contents

Abstract.....	2
Chapter 1: Introduction .....	3
1.1 Electromagnetic waves .....	3
1.2 Fresnel equations.....	6
1.3 Dielectric polarization .....	7
1.4 Permittivity.....	8
1.5 Kramers-Kronig relations .....	10
1.6 Excitons .....	11
1.7 Spectroscopic ellipsometry .....	13
1.8 Strontium Titanate .....	15
Chapter 2: Data Analysis Methodology .....	16
2.1 Experiment background.....	16
2.2 Experimental determination of the complex dielectric function .....	17
2.3 Curve Fitting of the complex dielectric function peaks .....	18
2.4 The curve fitting procedure .....	20
2.5 Kramers-Kronig transformations of the curves of best fit.....	27
Chapter 3: Results and Discussion .....	29
3.1 The curve fitting results .....	29
3.2 The Kramers-Kronig transformation results .....	36
Chapter 4: Conclusion & Future Work.....	42
4.1 Conclusion.....	42
4.2 Future work.....	43
References .....	44

## **Abstract**

Optical transitions play a role in the formation of excitons in Strontium Titanate (STO). It is known that the interband transitions between the valence band of STO to the conduction band of STO is the contributor of the Wannier excitons that are found in STO when a STO sample is irradiated with light. Resonant excitons in STO on the other hand, are the result of optical transitions between higher energy states. By curve fitting of the resonant excitonic peaks of the imaginary part of the temperature difference data of the complex dielectric function of STO obtained through spectroscopic ellipsometry and subsequently inputting the curve of best fit into the a Kramers-Kronig transformation, we obtain the corresponding “curve of best fit” for the real part of the temperature difference data of the complex dielectric function of STO. By comparing this result to the experimental data points of the real part of the temperature difference data of the complex dielectric function of STO, we deduce if the majority of the optical transitions between these higher energy states responsible for the resonant exciton are interband transitions. In addition, we also determine the sample quality of STO used in terms of the presence of impurities and defects via the curve fitting procedure.

# Chapter 1: Introduction

In this section, the background of spectroscopic ellipsometry, electromagnetic waves, behaviour of electromagnetic waves as they transit from one medium to another and of dielectrics in the presence of an applied external electric field is discussed. In addition, we discuss the various exciton types and a brief description of STO.

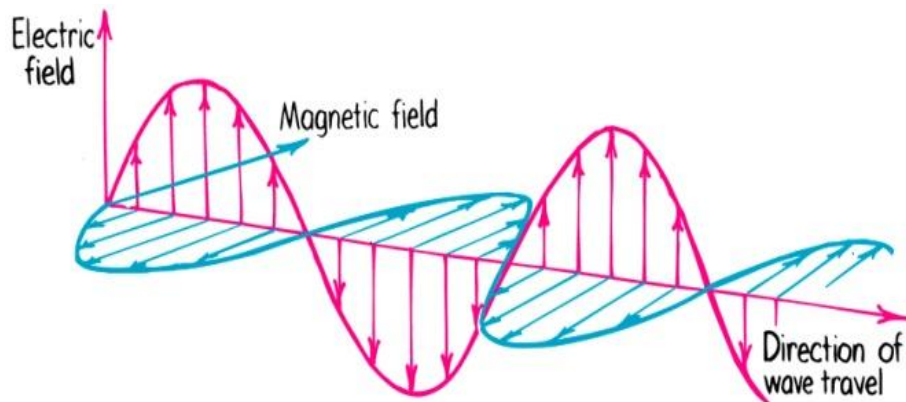
## 1.1 Electromagnetic waves

Electromagnetic waves travel at a constant speed, the speed of light in a vacuum or air medium. They arise from two oscillating electric and magnetic fields that oscillate about one another and are lying in planes perpendicular to each other. The wave propagation in three dimensional space for the oscillating electric field vector component  $\mathbf{E}$  and oscillating magnetic field vector component  $\mathbf{B}$  can be described by the following relations (1.1.1) and (1.1.2) respectively.

$$\mathbf{E} = \mathbf{E}_0 \exp[i(\omega t - \mathbf{k} \cdot \mathbf{r} + \delta)] \quad (1.1.1)$$

$$\mathbf{B} = \mathbf{B}_0 \exp[i(\omega t - \mathbf{k} \cdot \mathbf{r} + \delta)] \quad (1.1.2)$$

Here,  $\mathbf{E}_0$  is the amplitude of the electric field oscillation,  $\mathbf{B}_0$  is the amplitude of the magnetic field oscillation,  $\omega$  is the angular frequency,  $\mathbf{k}$  is the wave vector and  $\delta$  is the phase angle. The picture below illustrates the propagation of an electromagnetic wave.



Copyright © 2006 Paul G. Hewitt, printed courtesy of Pearson Education Inc., publishing as Addison Wesley.

Fig 1.1.1: An electromagnetic wave propagating in three dimensional space [1]

When light transits from a vacuum/air medium to a new medium that is of a higher density, it can be reflected, absorbed or transmitted through the new medium. The transmitted light travels at a speed lesser than the speed of light in the new denser medium. As a result, the light bends at the surface of the new denser medium, which is the interface between the vacuum/air medium and the new medium of higher density. This is a phenomenon known as refraction. The extent of refraction can be determined by the refractive index  $n$  which is defined by relation (1.1.3) below.

$$n = \frac{c}{v} \quad (1.1.3)$$

Here,  $c$  is the speed of light in a vacuum/air medium and  $v$  is the speed of light in the denser medium. When light transits from an initial medium call it medium one, to a new medium, call it medium two, the relation between the refractive indices of the mediums one and two can be related to one another by relation (1.1.4) below known as Snell's Law.

$$n_1 \sin \theta_1 = n_2 \sin \theta_2 \quad (1.1.4)$$

Here,  $n_1$  is the refractive index of medium one,  $\theta_1$  is the angle of incidence,  $n_2$  is the refractive index of medium two and  $\theta_2$  is the angle of refraction. The picture below shows the bending of light as it passes through the interface between two mediums of different densities, air and water.

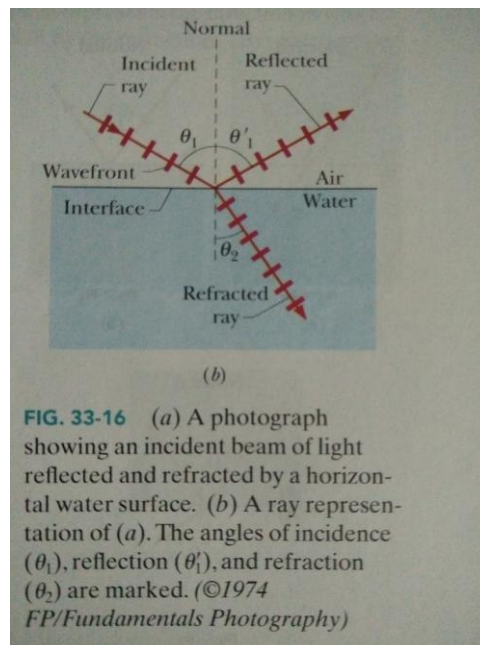


Fig 1.1.2: A light ray being refracted at the air-water interface [2]

When the refraction of light is accompanied by the attenuation of light as light passes through the optical medium, the refractive index is no longer a real value but a complex value.

In addition, electromagnetic waves obey Maxwell's equations [3]. The four of them are given below.

$$\nabla \cdot \mathbf{E} = \frac{\rho}{\epsilon_0} \quad (1.1.5)$$

$$\nabla \cdot \mathbf{B} = 0 \quad (1.1.6)$$

$$\nabla \times \mathbf{E} = -\frac{\partial \mathbf{B}}{\partial t} \quad (1.1.7)$$

$$\nabla \times \mathbf{B} = \mu_0 \left( \mathbf{J} + \epsilon_0 \frac{\partial \mathbf{E}}{\partial t} \right) \quad (1.1.8)$$

Here,  $\rho$  is the amount of charge enclosed by the Gaussian surface,  $\mathbf{J}$  is the amount of current density enclosed by the Amperian loop,  $\epsilon_0$  is the permittivity of free space and  $\mu_0$  is the permeability of free space. Equation (1.1.5) says that the amount of electric flux leaving a surface of an enclosed volume is proportional to the amount of charge enclosed inside the volume. Equation (1.1.6) says that no magnetic monopoles exist in nature. Equation (1.1.7) says that the amount of electromotive force induced in a closed loop is proportional to the rate of change of magnetic flux being enclosed by the loop. Finally, equation (1.1.8) says that the magnetic field generated around a closed loop is proportional to the sum of the electric current passing perpendicularly through the circular surface enclosed by the loop and the rate of change of electric flux being enclosed by the loop. Equations (1.1.5) and (1.1.6) are known as Gauss' Law for electric and magnetic monopoles respectively, equation (1.1.7) is known as Faraday's Law and equation (1.1.8) is known as Ampere's Law.

## 1.2 Fresnel equations

When light is polarized, it can either be p-polarized or s-polarized. “p” and “s” refer to its oscillating electric field lying on a plane that is parallel and perpendicular to the plane of incidence respectively.

The picture below illustrates the difference between light with “p” and “s” polarization.

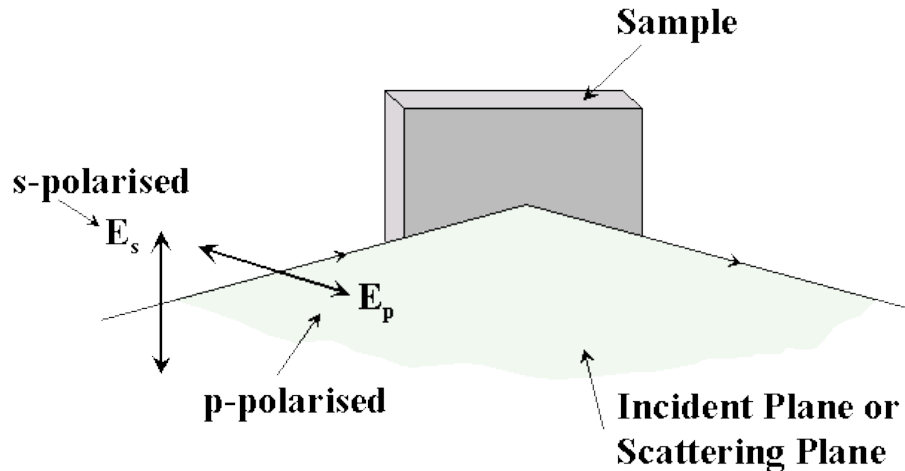


Fig 1.2.1: The p-polarized wave lies on the incident plane but the s-polarized wave is perpendicular to the incident plane [4]

The Fresnel equations describe the amount of reflection and transmission when light waves are incident on an interface between two different mediums. The reflection coefficient is the ratio of the amplitude of intensity of the reflected wave to that of the incident wave, while the transmission coefficient is the ratio of the amplitude of intensity of the transmitted wave to that of the incident wave.

The set of Fresnel equations that give the reflection coefficient for p-polarized  $r_p$  and s-polarized  $r_s$  light respectively are given below.

$$r_p = \frac{n_t \cos \theta_i - n_i \cos \theta_t}{n_t \cos \theta_i + n_i \cos \theta_t} \quad (1.2.1)$$

$$r_s = \frac{n_i \cos \theta_i - n_t \cos \theta_t}{n_i \cos \theta_i + n_t \cos \theta_t} \quad (1.2.2)$$



The set of Fresnel equations that give the transmission coefficient for p-polarized  $t_p$  and s-polarized  $t_s$  light respectively are given below.

$$t_p = \frac{2n_i \cos \theta_t}{n_t \cos \theta_i + n_i \cos \theta_t} \quad (1.2.3)$$

$$t_s = \frac{2n_i \cos \theta_i}{n_i \cos \theta_i + n_t \cos \theta_t} \quad (1.2.4)$$

Here,  $\theta_i$  is the angle of incidence,  $\theta_t$  is the angle of transmission,  $n_i$  is the refractive index of the medium the incident ray passes through and  $n_t$  is the refractive index of the medium the transmission ray passes through.

The Fresnel equations also apply to mediums with complex refractive indices.

### 1.3 Dielectric polarization

A dielectric material is in general a material where all charges are not free to move around the material like in conductors, but are tightly attached to their respective atoms or molecules. However, they are given some extent to move about within their respective atoms or molecules. When an external electric field is applied on a dielectric material, the positively charged nucleus and the negatively charged electron cloud within each atom or molecule experience an electric force in opposite directions causing them to move apart from each other in opposite directions. They move apart from each other until equilibrium is reached when the mutual forces of attraction holding them together are balanced by the forces of repulsion they experience as a result of the applied external electric field. This results in a slight shift of the positive charges in one direction and the negative charges in the opposite direction. Every atom or molecule possesses a small dipole moment as a result, which points in the opposite direction of the applied external electric field. The dielectric as a whole will have a net dipole moment pointing in the opposite direction of the applied external electric field contributed from the sum of all the small dipole moments of individual constituent atoms or molecules. This phenomenon is known as dielectric polarization. The extent of polarization is typically measured by the number of dipole moments per unit volume and is a vector quantity denoted by  $\mathbf{P}$ .

## 1.4 Permittivity

The permittivity of a dielectric material is a measure of the resistance encountered when an electric displacement field is generated in the material due to the application of an external electric field or in other words, the amount of electric displacement field that is generated in the material due to the application of an external electric field. For an instantaneous response of a dielectric material to an applied external electric field, the electric displacement in the material  $\mathbf{D}$  due to the application of the external electric field  $\mathbf{E}$  is given by relation (1.4.1) below.

$$\mathbf{D} = \varepsilon \mathbf{E} \quad (1.4.1)$$

Here,  $\varepsilon$  is the permittivity. It is a scalar for an isotropic medium but a tensor for an anisotropic medium. In addition it can also be a function of position, frequency of the applied external electric field for oscillating applied fields and other physical parameters. The electric displacement in the material  $\mathbf{D}$  due to the application of the external electric field  $\mathbf{E}$  can alternatively be expressed in terms of the applied external electric field  $\mathbf{E}$  and the polarization  $\mathbf{P}$  by relation (1.4.2) below.

$$\mathbf{D} = \varepsilon_0 \mathbf{E} + \mathbf{P} \quad (1.4.2)$$

For many dielectric mediums, the polarization  $\mathbf{P}$  is directly proportional to the applied external electric field [5] which can be expressed by relation (1.4.3) below.

$$\mathbf{P} = \varepsilon_0 \chi \mathbf{E} \quad (1.4.3)$$

Here,  $\chi$  is called the susceptibility which is a measure of how easily polarization occurs for a particular dielectric medium subject to an external electric field. After substituting (1.4.3) into (1.4.2), we can express the electric displacement in the material  $\mathbf{D}$  by relation (1.4.4) below.

$$\mathbf{D} = \varepsilon_0 (1 + \chi) \mathbf{E} \quad (1.4.4)$$

By comparing (1.4.1) and (1.4.4), we find that the permittivity is related to the susceptibility by relation (1.4.5) below.

$$\varepsilon = \varepsilon_0 (1 + \chi) \quad (1.4.5)$$

Physically, this means that when a particular dielectric medium polarizes more easily, the lesser the resistance encountered when an electric displacement field is generated in the material due to the application of an external electric field.

In reality, an instantaneous response of a dielectric material to an applied external electric field is unrealistic. Naturally, there is a response time or time lag to dielectric polarization which would imply a non-instantaneous response rather than an instantaneous response. In order to model such non-instantaneous response, we need to replace the permittivity that can only take on real values with a complex permittivity that can take on complex values. This is because the phase difference of a complex value can be used to represent a delay in response, that is, the dielectric polarization depends on the external electric field applied in the past. The complex permittivity is defined by the complex number which can be given by relation (1.4.6) below.

$$\varepsilon = \varepsilon_1 + i\varepsilon_2 \quad (1.4.6)$$

In the case that there is instantaneous response, the imaginary part of the complex value is zero and hence the complex permittivity is only given by the real part of the complex value and so the complex permittivity reduces to the original definition of permittivity as discussed previously which is a real value. In terms of the physical meaning, the real part of the complex permittivity is related to the energy stored in the medium due to dielectric polarization and the imaginary part of the complex permittivity is related to the energy absorbed by the medium and lost to heat or other forms of energy. The complex permittivity can be referred to as a dielectric function of angular frequency  $\omega$  when the applied external electric field is oscillating with angular frequency  $\omega$ , with the real and imaginary parts both being functions of the angular frequency  $\omega$ .

## 1.5 Kramers-Kronig relations

The real part of the dielectric function is related to the complex part of the dielectric function and vice versa. The Kramers-Kronig relations are a pair of integral formulas that describe the mathematical connection between the two functions. They are given below.

$$\varepsilon_1(\omega) = \frac{1}{\pi} P.V. \int_{-\infty}^{\infty} \frac{\omega' \varepsilon_2(\omega')}{\omega'^2 - \omega^2} d\omega' \quad (1.5.1)$$

$$\varepsilon_2(\omega) = -\frac{1}{\pi} P.V. \int_{-\infty}^{\infty} \frac{\varepsilon_1(\omega') - 1}{\omega'^2 - \omega^2} d\omega' \quad (1.5.2)$$

P.V. denotes the Cauchy principal value. For a function that is to be integrated but has a singularity existing in between its lower and upper limits, the Cauchy principal value enables the integral to be evaluated to a real value for an integral which would otherwise be undefined. The definition of the Cauchy principal value is given by relation (1.5.3) below.

$$P.V. \int_a^b f(x) dx = \lim_{\epsilon \rightarrow 0^+} \left[ \int_a^{c-\epsilon} f(x) dx + \int_{c+\epsilon}^b f(x) dx \right] \quad (1.5.3)$$

Once one knows the complex part of the dielectric function for all frequencies, one can obtain the real part of the dielectric function for all frequencies through the Kramers-Kronig relations and vice versa.

## 1.6 Excitons

When a light photon is absorbed by an optical medium, exciting an electron from the valence band to the conduction band, a hole is created in the valence band. An electron-hole pair is formed. If the electron-hole pair does not recombine, they are held together by Coulomb attraction due to the positive charge on the hole and the negative charge on the electron analogous to that of the hydrogen atom. This electron-hole pair taken together as a single particle is known as an exciton. There are two well known types of exciton, one type being the Wannier exciton and the other being the Frenkel exciton.

The Wannier type exciton has its electron weakly bound to its hole. Hence, there is a large average electron-hole distance. The binding energy is approximately 10meV and the atomic radius is approximately  $100\text{\AA}$ . The exciton is also delocalized from the atom of origin and is free to move around the crystal structure. Wannier type excitons are typically found in semiconductors.

The Frenkel type exciton has its electron tightly bound to its hole. Hence, there is a small average electron-hole distance. The binding energy is approximately 1eV and the atomic radius is approximately  $10\text{\AA}$ . The exciton is also localized to the atom of origin. However, it is able to move through the crystal structure by hopping from atom to atom in a wavelike manner. Frenkel type excitons are typically found in alkali halides and organic materials. The picture below compares a Wannier type exciton and a Frenkel type exciton in a crystal lattice.

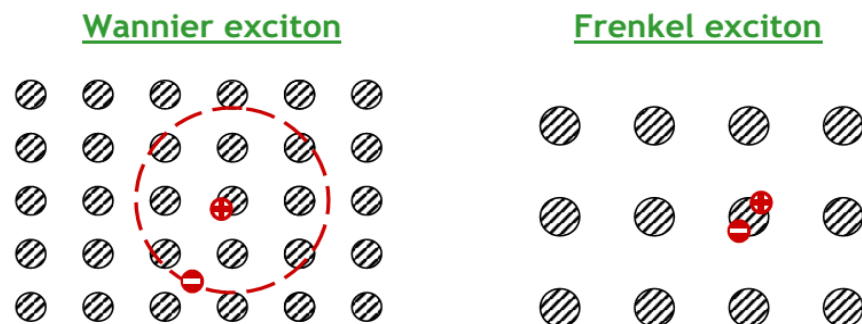


Fig 1.6.1: The difference between a Wannier type and Frenkel type exciton [6]

In semiconductors, the exciton energy levels are all just below the direct band gap of the conduction band for Wannier type excitons. These are where the electronic part of the exciton resides.

The picture below illustrates this.

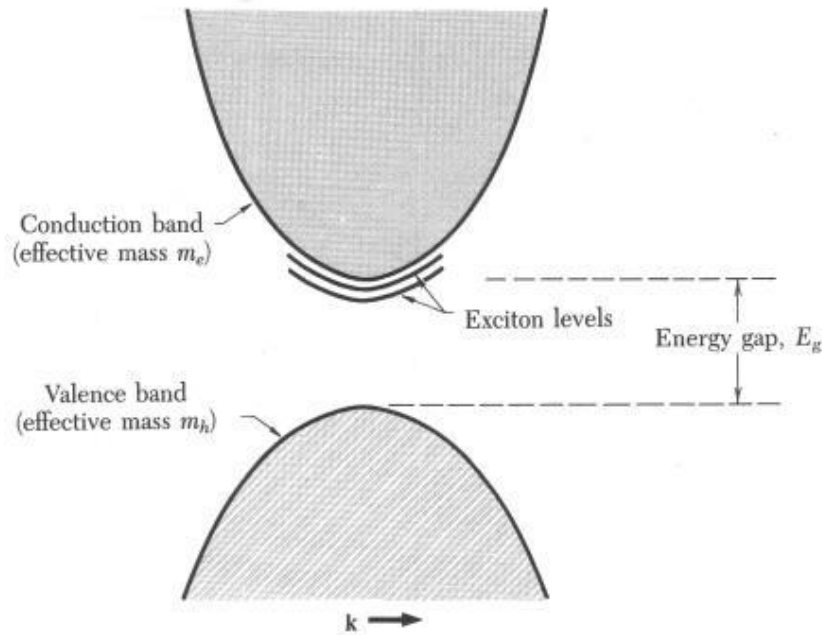


Fig 1.6.2: The exciton levels a Wannier type exciton in a semiconductor

Electron-electron and electron-hole pairs can interact with one another due to Coulomb forces of attraction and repulsion in a many body problem. When both the electron-electron and electron-hole interactions are strongly coupled, it can give rise to a novel type of exciton termed as the resonant exciton. Unlike the Wannier excitons, resonant excitons occur at higher energy bands and they can occur at energies well above the corresponding optical band gap of the material [7]. This is a relatively new phenomenon that has yet to be studied in detail. A suggested useful tool to experimentally probe such resonant excitons is via spectroscopic ellipsometry.

## 1.7 Spectroscopic ellipsometry

Spectroscopic ellipsometry is an experimental technique that studies the change in polarized light upon the reflection and transmission of light in an optical medium. The measured optical properties of the medium are the amplitude ratio  $\psi$  and the phase difference  $\Delta$  between the p-polarized and s-polarized light waves. Spectroscopic ellipsometry is typically carried out in the infrared-visible to ultraviolet region. Spectroscopic ellipsometry measures the  $(\psi, \Delta)$  spectra across a continuous range of incident photon energies  $h\nu$ . Here,  $h$  is the Planck's constant and  $\nu$  is the frequency of the incident photon. Subsequently, an optical model that assumes the medium has a perfectly flat surface and infinite thickness is employed to obtain the pseudo dielectric function (PDF)  $\langle \varepsilon \rangle$  directly from the  $(\psi, \Delta)$  spectra. If the medium is isotropic and atomically flat, then the PDF  $\langle \varepsilon \rangle$  approaches the true dielectric function  $\varepsilon$ . Spectroscopic ellipsometry plays an important role in the study of excitonic effects as it is able to probe neutral excitations that give rise to electron-hole pairs and excitons.

The complex reflectance ratio  $\rho_r$  is defined by relation (1.7.1) below.

$$\rho_r = \frac{r_p}{r_s} \quad (1.7.1)$$

When light reflection is measured in spectroscopic ellipsometry, the amplitude ratio  $\psi_r$  and the phase difference  $\Delta_r$  between the p-polarized and s-polarized light waves are related to the complex reflectance ratio by relation (1.7.2) below.

$$\rho_r = \tan(\psi_r) \exp(i\Delta_r) \quad (1.7.2)$$

Here,  $\psi_r$  is the amplitude ratio between the reflected p-polarized and s-polarized light waves and  $\Delta_r$  is the phase difference between the reflected p-polarized and s-polarized light waves.

The PDF can be obtained by relation (1.7.3) below.

$$\langle \varepsilon \rangle = \sin^2 \theta_i \left[ 1 + \tan^2 \theta_i \left( \frac{1 - \rho_r}{1 + \rho_r} \right) \right] \quad (1.7.3)$$

Here,  $\theta_i$  is the angle of incidence of the light beam which is pre-determined in the spectroscopic ellipsometry experiment and  $\rho_r$  is the complex reflectance ratio which can be found directly using (1.7.2) with values obtained from the  $(\psi_r, \Delta_r)$  spectra which is measured during the spectroscopic ellipsometry experiment. Assuming the medium used in the spectroscopic ellipsometry experiment to be isotropic and atomically flat, the true dielectric function  $\epsilon$  can be considered to be equivalent to the PDF  $\langle \epsilon \rangle$  and can hence be given by (1.7.3).

General restrictions that have to be imposed on the optical medium being used for spectroscopic ellipsometry are that the surface roughness of the sample is small and the measurements have to be conducted at an oblique incidence. The rationale for the former being that the light scattered by a rough surface reduces the reflected light intensity severely, rendering the polarization state difficult to measure. The rationale for the latter being that at normal incidence, p-polarized and s-polarized waves cannot be distinguished making measurements of the polarization state impossible [8].

The picture below shows how spectroscopic ellipsometry works.

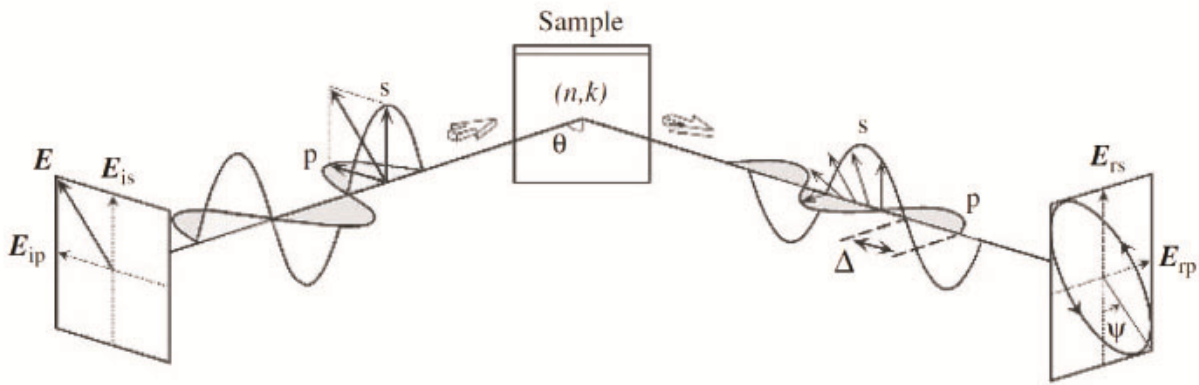


Fig 1.7.1: Spectroscopic ellipsometry on a sample

A beam of light is incident on the medium at a fixed angle of incidence  $\theta$ . The medium has an intrinsic refractive index  $n$  which affects the amplitude ratio  $\psi$  and extinction coefficient  $k$  which affects the phase difference  $\Delta$ . The reflected light is measured by a detector which records the  $(\psi_r, \Delta_r)$  spectra across a continuous range of incident photon energies.



## 1.8 Strontium Titanate

Strontium titanate (STO) is a perovskite-type titanate. A perovskite is a material that has the same crystal structure as calcium titanate. A perovskite has a general chemical formula  $ABX_3$  where A and B represent cations of different sizes and X is an anion.

The crystal structure of STO is shown in the picture below.

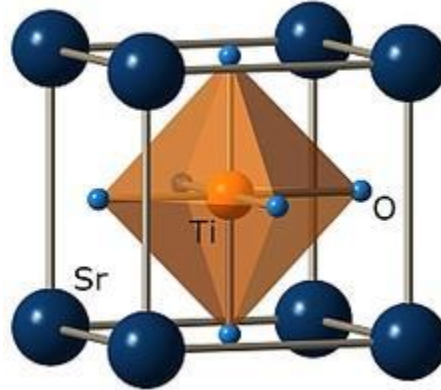


Fig 1.8.1: The crystal structure of STO or a perovskite in general [9]

The Wannier exciton in STO has its electronic part well localized on the Ti atom, while the hole is localized on the neighbouring O atom [10]. STO has a band gap of 3.2eV separating the valence and conduction band at zero Kelvin [11]. The six fold coordination of Ti ions by surrounding O ions result in a crystal field splitting of the degenerate Ti-3d states at 2.4eV into two states Ti-3d  $t_{2g}$  and Ti-3d  $e_g$ . Speaking in terms of bands, the valence band of STO which is the band with highest occupied molecular orbitals is the mainly the O-2s and O-2p states of oxygen and the conduction band which is the band with lowest unoccupied molecular orbitals is mainly the titanium empty Ti-3d states of titanium.

There are all together three excitonic peaks for STO named Ex1, Ex2 and Ex3. The Ex1 peak at 3.75eV at 4.2K is identified as a Wannier excitonic peak while the Ex2 and Ex3 peaks at 4.67eV and 6.11eV respectively at 4.2K are identified as resonant excitonic peaks [12].

## **Chapter 2: Data Analysis Methodology**

In this section, we will discuss a brief overview of the spectroscopic ellipsometry procedure used to generate the data that is being collected for the data analysis. We will then discuss the curve fitting procedure with the aid of Mathematica for the temperature difference of the imaginary component of the complex dielectric function of STO. This will be followed by a discussion on the application of the Kramers-Kronig relations on the curve fitted function of the temperature difference of the imaginary component of the complex dielectric function to obtain the graph of the temperature difference of the real component of the complex dielectric function of STO with the aid of Mathematica. Last but not least, the graph of the temperature difference of the real component of the complex dielectric function generated from the above procedure is compared to the experimental data of the temperature difference of the real component of the complex dielectric function of STO for analysis.

### **2.1 Experiment background**

STO (100) samples from Crystec are being used for the spectroscopic ellipsometry measurements. They are all of size 10mm by 10mm by 0.5mm and single side polished with rms roughness less than 5Å. Spectroscopic ellipsometry is carried out with a commercial rotating analyser ellipsometer from J.A. Woollam Inc which covers a photon energy range from 0.6eV to 6.5eV in steps of 0.02eV. The lowest temperature that the STO samples are at is 4.2K and the highest temperature that the STO samples are at is 350K. The low temperature measurements are carried out in an open cycle cryostat with base pressures within the regime of  $10^{-9}$  Torr, created by a mixture of liquid helium and liquid nitrogen. The angle of incidence for all measurements made by the cryostat is fixed at 70°.

## **2.2 Experimental determination of the complex dielectric function**

The STO samples are measured in air. Hence, the optical model employed is an air-sample interface. The optical model also assumes a sample of infinite thickness. This assumption is valid as the depth of the STO sample is much greater than the light beam penetration depth which does not exceed  $1\ \mu\text{m}$ . In addition, the optical model assumes an atomically flat surface which is valid because all the STO samples have rms roughness less than  $5\text{\AA}$ . Hence, the PDF which is experimentally obtained directly from the spectroscopic ellipsometry measurements can be considered to be the true complex dielectric function of STO.

## 2.3 Curve Fitting of the complex dielectric function peaks

The analysis of the peak data points obtained from spectroscopic ellipsometry requires knowledge of the dielectric function pertaining to the sample. However, we do not know the dielectric functions pertaining to the sample. We attempt to curve fit the peaks with bell-shaped distributions, namely the Gaussian, Lorentz and Voigt profile.

We curve fit the imaginary component of the complex dielectric function as it is the imaginary component that is dependent on the energy absorption of the material, which is in turn linked to the material's behavior in terms of photon absorption in order to form the exciton.

The Gaussian profile is a Gaussian distribution defined by relation (2.3.1) below.

$$G(x) = A \exp\left(-\frac{(x - B)^2}{C^2}\right) \quad (2.3.1)$$

Here,  $A, B$  and  $C$  are parameters that describe the height of the peak, the  $x$  position and the standard deviation of the bell-shaped curve of the Gaussian distribution respectively. Note that the standard deviation is related to the half-width at half-maximum of the bell-shaped curve of the Gaussian distribution.

The Lorentz profile is a Cauchy distribution defined by relation (2.3.2) below.

$$L(x) = \frac{AC^2}{(x - B)^2 + C^2} \quad (2.3.2)$$

Here,  $A, B$  and  $C$  are parameters that describe the height of the peak, the  $x$  position and the scale parameter determining the half-width at half-maximum of the bell-shaped curve of the Cauchy distribution respectively. It is worth to mention that the Lorentz profile looks like a Gaussian profile with a bell-shape but with lighter tails, that is, tails that go down less rapidly.

The Voigt profile is a profile that is obtained from the convolution of the Gaussian profile and the Lorentz profile. The Voigt profile is defined by relation (2.3.3) which follows where the asterisk is the notation for a convolution operation.

$$V(x) = (G * L)(x) = \int_{-\infty}^{\infty} G(x)L(x-t)dt \quad (2.3.3)$$

For the convenience of computation, the Voigt profile is often approximated by the pseudo-Voigt profile which is much easier to work with [13]. The pseudo-Voigt profile is given by the linear combination of or a weighted sum of the Gaussian and Lorentz profiles. The pseudo-Voigt profile is defined by relation (2.3.4) below.

$$V_{Pseudo}(x) = \eta G(x) + (1 - \eta)L(x) \quad (2.3.4)$$

Here,  $\eta$  and  $1 - \eta$  are the weights attached to the Gaussian profile and the Lorentz profile respectively and they must both sum to unity and hence,  $\eta$  is a value that must be bounded below by zero and bounded above by one. In addition, the parameters  $A, B$  and  $C$  in the pseudo-Voigt profile must be same for both the Gaussian profile and the Lorentz profile involved.

## 2.4 The curve fitting procedure

The experimental data of the temperature difference of the imaginary component and real component of the complex dielectric function of STO is obtained from the Singapore Synchrotron Light Source (SSLS). The temperature difference of the imaginary component of the complex dielectric function is defined by relation (2.4.1) that follows.

$$\delta_T \langle \varepsilon_i \rangle = \langle \varepsilon_i \rangle(T) - \langle \varepsilon_i \rangle(350K) \quad (2.4.1)$$

Here,  $i$  takes the value 1 for the real component and the value 2 for the imaginary component.  $T$  is the temperature the STO samples are at when the measurements are taken in Kelvin. The curve fitting procedure is done on the experimental data of the temperature difference of the imaginary component ( $i = 2$ ) at  $T = 4.2K$ ,  $T = 50K$ ,  $T = 200K$  and  $T = 325K$ . The curve fitting procedure can be categorized into three main steps.

Step 1: Plotting of the data plots in Mathematica.

The experimental data of the temperature difference of the imaginary component at  $T = 4.2K$ ,  $T = 50K$ ,  $T = 200K$  and  $T = 325K$  are imported into the Mathematica software via a CSV version of the original excel file. The Mathematica command for the procedure using  $T = 4.2K$  as an example is as follows:

- `Import["E:\\csv Fig1(c) delta T epsilon 2 4.2K.csv"]`

The data plots of the  $\delta_T \langle \varepsilon_2 \rangle$  against incident photon energy in electron volts are then plotted for the various temperatures. The Mathematica command for the procedure using  $T = 4.2K$  as an example is as follows:

- `ListPlot[{{6.5,0.0667}, ..., {0.6,0.008986}}]`

Here,  $\{6.5,0.0667\}, \dots, \{0.6,0.008986\}$  are all the data points imported from the csv file by evaluating the “Import” command.

The data plot using  $T = 4.2K$  as an example is shown below.

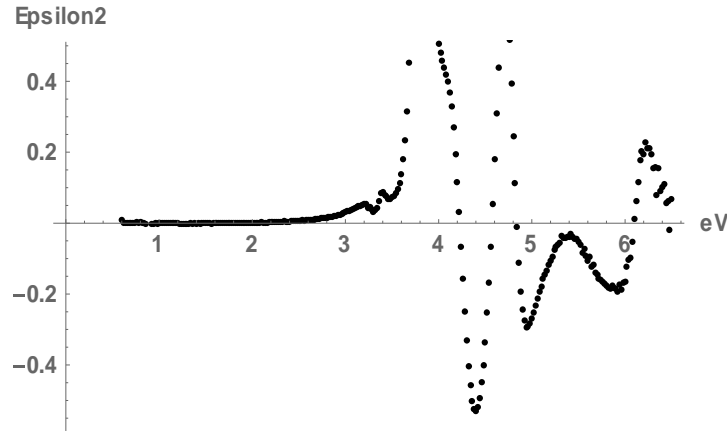


Fig 2.4.1: The data plot for  $\langle \varepsilon_2 \rangle$  across the whole range of photon energies

Step 2: Zooming into the photon energy neighbourhood of the excitonic peak in order to find the location of the peak data point.

There are all together three excitonic peaks for STO, Ex1, Ex2 and Ex3.

For each peak, there is a corresponding peak data point that is very close to the true peak. The photon energy neighbourhood for which the peak data point has  $\delta_T \langle \varepsilon_2 \rangle$  value that is the local maximum of all  $\delta_T \langle \varepsilon_2 \rangle$  values of all the data points within the neighbourhood is determined. This can be done by referring to the data plot generated in step 1.

The data plot of  $\delta_T \langle \varepsilon_2 \rangle$  against photon energy restricted to the photon energy neighbourhood determined is then plotted. The Mathematica command for the procedure using  $T = 4.2K$  for the Ex1 peak as an example is as follows:

- `ListPlot[{{4.5, -0.336}, ..., {3.5, 0.07305}}]`

Here,  $\{4.5, -0.336\}, \dots, \{3.5, 0.07305\}$  are all the data points chosen to be in the restricted neighbourhood of photon energy.

The data plot using  $T = 4.2K$  for the Ex1 peak as an example is shown below.

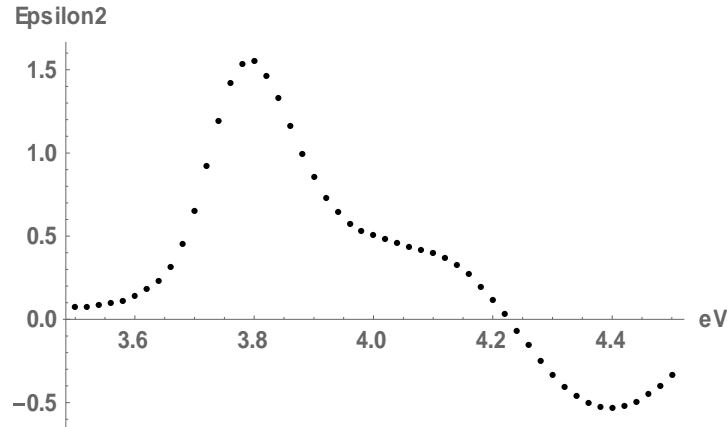


Fig 2.4.2: The data plot for  $\langle \varepsilon_2 \rangle$  within the neighbourhood of the Ex1 peak

The photon energy and the  $\delta_T \langle \varepsilon_2 \rangle$  values corresponding to the peak data point are then found. The Mathematica command for the procedure using  $T = 4.2K$  for the Ex1 peak as an example is as follows:

- `MaximalBy[{{4.5, -0.336}, ... , {3.5, 0.07305}}, Last]`

The “MaximalBy” command picks out the data point that has the largest  $\delta_T \langle \varepsilon_2 \rangle$  value within the restricted neighbourhood of photon energy when evaluated. This corresponds to the peak data point. The Mathematica output is shown below.

➤ `{{3.8, 1.5513}}`

Step 3: Finding the curve of best fit.

The sum of square error (SSE) is defined by relation (2.4.1) below.

$$SSE = \sum_{i=1}^n (\widehat{\delta_T \langle \varepsilon_2 \rangle}_i - \delta_T \langle \varepsilon_2 \rangle_i)^2 \quad (2.4.1)$$

Here,  $\widehat{\delta_T \langle \varepsilon_2 \rangle}_i$  is the estimated value from the curve of fit and  $\delta_T \langle \varepsilon_2 \rangle_i$  is the value from the experimental data point, while  $i$  labels the data points and  $n$  is the total number of data points used in the curve fitting.



The mean square error (MSE) is defined by relation (2.4.2) below.

$$MSE = \frac{SSE}{n} \quad (2.4.2)$$

For a particular type of curve with variable parameters, the curve of best fit is attained when the MSE is minimized. Knowing the values of the respective parameters when the MSE is minimized will give the equation of the curve of best fit. The process of obtaining the equation of the curve of best fit can be split into two cases. When curve fitting any peak, we may assume case 1. If case 1 does not suffice, then we proceed to case 2.

For each peak, we start by finding the equation of the curve of best fit for the Gaussian and Lorentz profile respectively. We guess that the parameters  $A$  and  $B$  respectively take the values of  $\delta_T\langle\varepsilon_2\rangle$  and the photon energy of the corresponding peak data point found previously in step 2. For the  $C$  parameter, we start by setting it to take the value of 0.1. Starting from the corresponding peak data point found previously in step 2, 10 data points to its left and 10 data points to its right are chosen. Any data points that have negative  $\delta_T\langle\varepsilon_2\rangle$  value are discarded as these are in the invalid range of values for a Gaussian or Lorentz profile.

Next, we find the equation of the curve of best fit for the Gaussian and Lorentz profile respectively. The Mathematica commands for the procedure using  $T = 4.2K$  for the Ex1 peak as an example for the Gaussian and Lorentz profile respectively are as follows:

- FindFit[{{4.,0.5069}, ..., {3.6,0.1389}}, aExp[-(1 / 2)((x - b)^2) / (c^2)], {{a, 1.5513}, {b, 3.8}, {c, 0.1}}, x]
- FindFit[{{4.,0.5069}, ..., {3.6,0.1389}}, a ((c^2)) / (((x - b)^2 + c^2)), {{a, 1.5513}, {b, 3.8}, {c, 0.1}}, x]

For all the curve fittings done, it has been observed that the  $C$  parameter of every curve of best fit for the Gaussian or Lorentz profile always takes values close to 0.1. Hence, it suffices to use 0.1 as a guess for all curve fittings involving the Gaussian and Lorentz profile. Furthermore, since the pseudo Voigt profile is a linear combination of the Gaussian and Lorentz profile, we expect the  $C$  parameter of every curve of best fit for the pseudo Voigt profile to take values close to 0.1 as well.

Case 1: The unconstrained pseudo Voigt profile suffices.

For each peak, we start by trying to curve fit the pseudo Voigt profile. We guess that the parameters  $A$  and  $B$  respectively take the values of  $\delta_T\langle\varepsilon_2\rangle$  and the photon energy of the corresponding peak data point found previously in step 2 and the  $C$  parameter takes the value 0.1. We initially fix the  $\eta$  parameter to take the value of 0.5. That is, assuming half Gaussian and half Lorentz profile. Starting from the corresponding peak data point found previously in step 2, 10 data points to its left and 10 data points to its right are chosen. Any data points that have negative  $\delta_T\langle\varepsilon_2\rangle$  value are discarded as these are in the invalid range of values for a pseudo Voigt profile.

Next, we find the equation of the curve of best fit for a pseudo Voigt profile. The Mathematica command for the procedure using  $T = 4.2K$  for the Ex1 peak as an example are as follows:

- `FindFit[{{4.,0.5069}, ..., {3.6,0.1389}}, (d)(aExp[-(1/2)((x - b)^2/c^2])) + (1 - d)(a(c^2)/((x - b)^2 + c^2)), {{a, 1.5513}, {b, 3.8}, {c, 0.1}, {d, 0.5}}, x]`

Here,  $\{4.,0.5069\}, \dots, \{3.6,0.1389\}$  are all the data points chosen for the curve fitting, and  $a, b, c$  and  $d$  are the parameters of the pseudo Voigt profile. The “FindFit” command picks out the particular values of the parameters that give the pseudo Voigt profile with the minimum MSE and hence gives the equation of the curve of best fit for the pseudo Voigt profile. The Mathematica output is shown below.

- `{a → 1.5474037950439945, b → 3.809141821065091, c → 0.09653023488528577, d → 0.3288744821908265}`

Only the  $\eta$  parameter that needs to be varied when guessed. The  $\eta$  parameter is bounded below by 0 and above by 1. As a rule of thumb, we can first guess the  $\eta$  parameter to take the value of 0.5. Should unreasonable estimates of any of the parameters be obtained, we guess the  $\eta$  parameter again in increasing or decreasing steps of 0.1. In the case of the  $T = 4.2K$  Ex1 peak example, the guessed parameter values all turn out to be close to the parameter values that give the minimum MSE and hence, a reasonable answer is obtained immediately.

Case 2: The unconstrained pseudo Voigt profile does not suffice.

In this case, regardless of the guessed  $\eta$  parameter value, the estimated value of  $\eta$  that gives the minimum MSE violates the bounded range of  $\eta$ . There are three possible scenarios for this. 1) A pure Gaussian fit is better than a pseudo Voigt fit. 2) A pure Lorentz fit is better than a pseudo Voigt fit. 3) There exists a pseudo Voigt fit subject to specific parameter constraints which is better than a pure Gaussian fit or a pure Lorentz fit. In such a case we use equation of the curve of best fit for the Gaussian and Lorentz profile respectively found earlier. The Mathematica commands for the procedure using  $T = 4.2K$  for the Ex2 peak as an example are as follows:

- `FindFit[{{4.82,0.1134}, ..., {4.58,0.0542}}, aExp[-(1 / 2)((x - b)^2) / (c^2)], {{a, 0.6769}, {b, 4.7}, {c, 0.1}}, x]`
- `FindFit[{{4.82,0.1134}, ..., {4.58,0.0542}}, a ((c^2)) / (((x - b)^2 + c^2)), {{a, 0.6769}, {b, 4.7}, {c, 0.1}}, x]`

Here,  $\{4.82,0.1134\}, \dots, \{4.58,0.0542\}$  are all the data points chosen for the curve fitting and  $a$ ,  $b$  and  $c$  are the parameters of the Gaussian or Lorentz profile. The Mathematica output for the Gaussian and Lorentz profiles respectively are shown below.

- `{a → 0.6998666748112617, b → 4.706298030956792, c → 0.06502387531432574}`
- `{a → 0.7236937073529958, b → 4.706798920242006, c → 0.0711351185744713}`

The respective parameter estimates obtained from the Gaussian and Lorentz curves of best fit are then used as the upper and lower parameter limits in the constrained pseudo Voigt profile curve fitting. The Mathematica commands for the procedure using  $T = 4.2K$  for the Ex2 peak as an example are as follows:

- `FunctiontableEx2 = Table[(d)(aExp[-(1/2)((i - b)^2/c^2])) + (1 - d)(a (c^2)/((i - b)^2 + c^2)), {i, 4.58,4.82,0.02}]`
- `DatatableEx2 = DataEx2cleaned[[All, 2]]`
- `ErrorableEx2 = (FunctiontableEx2 - DatatableEx2)^2`

- $MSEEx2 = (1/13)Total[\left\{\left(-0.1134 + \frac{ac^2(1-d)}{(4.58-b)^2+c^2} + ade^{-\frac{(4.58-b)^2}{2c^2}}\right)^2, \dots, \left(-0.0542 + \frac{ac^2(1-d)}{(4.82-b)^2+c^2} + ade^{-\frac{(4.82-b)^2}{2c^2}}\right)^2\right\}]$
- $NMinimize[MSEEx2, \{0.699867 < a < 0.723694, 4.7063 < b < 4.7068, 0.0650239 < c < 0.0711351, 0 < d < 1\}, \{a, b, c, d\}]$

Here, FunctiontableEx2 refers to the set of values of  $\widehat{\delta_T\langle\varepsilon_2\rangle}_i$  in (2.4.1) and DatatableEx2 refers to the set of values of  $\delta_T\langle\varepsilon_2\rangle_i$  in (2.4.1). The set of values of  $(\widehat{\delta_T\langle\varepsilon_2\rangle}_i - \delta_T\langle\varepsilon_2\rangle_i)^2$  in (2.4.1) is given by ErrortableEx2 and the MSE is given by MSEEx2 which is obtained by summing all the elements in the ErrortableEx2 set divided by the total number of data points which is 13 in this example. The “NMinimize” command picks out the particular values of the parameters that give the pseudo Voigt profile with the minimum MSE subject to the upper and lower limits set on the parameters. The operation of the “NMinimize” command here in case 2 is essentially the same as the “FindFit” command in case 1 with the difference that all the parameters are subjected to constraints, whereas in case 1, the parameters are not subjected to any constraints. The Mathematica output is shown below.

- $\{0.004437800402261194, \{a \rightarrow 0.699867, b \rightarrow 4.7063, c \rightarrow 0.06553247217677842, d \rightarrow 0.9999999886667468\}\}$

If the  $\eta$  parameter takes a value that tends to 1, then it implies scenario 1). On the other hand, if the  $\eta$  parameter takes a value that tends to 0, then it implies scenario 2). Lastly if the  $\eta$  parameter takes a value that is in between 0 and 1, then it implies scenario 3). This example fits scenario 1). The pure Gaussian curve of best fit is the best curve that can be fitted as compared to the pure Lorentz curve or the pseudo Voigt curve of best fits.

## 2.5 Kramers-Kronig transformations of the curves of best fit

For each peak, after obtaining the curve of best fit from the curve fitting procedure, the substitution  $\omega = E/h$  is used where  $E$  is the photon energy converted from electron volts to Joules and  $h$  is the Planck's constant in the integration that results from the application of (1.5.1) on the curve of best fit in order to obtain the corresponding relationship of the temperature difference of the real component of the complex dielectric function of STO against the frequency of the incident photons. Due to the Cauchy principal value of the integral not having a closed form, a graph that describes the relationship is obtained for each peak. The Mathematica command for the procedure using  $T = 4.2K$  for the Ex1 peak as an example are as follows:

- `Plot[NIntegrate[(2.4177)(x / Pi)((0.328874)(1.5474Exp[-(1 / 2)((x - 9.2105)^2] / (0.0965302^2)))] + (1 - 0.328874)(1.5474 ((0.0965302^2)) / (((x - 9.2105)^2 + 0.0965302^2)))] / ((x^2 - w^2)), {x, 8.7048, w, 9.672}, Method -> {"PrincipalValue"}], {w, 8.7049, 9.6719}]`

The “NIntegrate” command gives the best approximation to the integral arising from (1.5.1) at every value of photon frequency within the valid range and the “Plot” command plots out the graph.

The temperature difference data of the real component at  $T = 4.2K$ ,  $T = 50K$ ,  $T = 200K$  and  $T = 325K$  is given in terms of  $\delta_T\langle\varepsilon_1\rangle$  against incident photon energy in electron volts. It has to be converted into  $\delta_T\langle\varepsilon_1\rangle$  against frequency of the incident photons so that the data points when plotted can be directly compared with the graph obtained via the Kramers-Kronig transformation. This conversion is done to the temperature difference data of the real component at  $T = 4.2K$ ,  $T = 50K$ ,  $T = 200K$  and  $T = 325K$  in the relevant CSV files before being imported into the Mathematica software. The data plots of the  $\delta_T\langle\varepsilon_1\rangle$  against incident photon frequency in  $10^{14}$  Hertz are then plotted for the various temperatures. The Mathematica command for the procedure using  $T = 4.2K$  for the Ex1 peak as an example is as follows:

- `ListPlot[{{9.6708, -0.5788}, ... , {8.70372, 0.6125}}]`

We then compare the graph obtained for the temperature difference of the real component via the Kramers-Kronig transformation of the fitted curve with the experimental data points for the temperature difference of the real component.

## Chapter 3: Results and Discussion

In this section, we will discuss the physical insight that we can gain from the curve fitting results of the experimental data points of the temperature difference of the imaginary component of the complex dielectric function and the results of the Kramers-Kronig transformation on the curve fitted results. By considering the temperature difference of the imaginary component in (2.4.1), we are assuming that interband transitions do not exist in the formation of the resonant exciton. By performing the curve fitting and subsequently comparing the Kramers-Kronig transformation of the best fit curve to the experimental data points of the real component of the complex dielectric function, we should be able to tell if this assumption is valid for the resonant exciton.

### 3.1 The curve fitting results

The following table shows the respective curves of best fit and the corresponding excitonic peaks in the temperature difference data of the imaginary component of the complex dielectric function across the different temperatures.

Excitonic Peak	Temperature	Curve of Best Fit	A Parameter	B Parameter	C Parameter	D Parameter
Ex1	4.2K	Pseudo-Voigt	1.54740	3.80914	0.0965302	0.328874
Ex2	4.2K	Pure Gaussian	0.699867	4.70630	0.0650239	-
Ex3	4.2K	Pure Gaussian	0.211112	6.24982	0.102759	-
Ex1	50K	Pseudo-Voigt	1.46836	3.81599	0.0962429	0.437108
Ex2	50K	Pure Gaussian	0.678594	4.71109	0.0641915	-
Ex3	50K	Pure Gaussian	0.175823	6.26828	0.112125	-

Ex1	200K	Pseudo-Voigt	0.715669	3.86117	0.106052	0.637435
Ex2	200K	Pure Gaussian	0.347736	4.74147	0.0733798	-
Ex3	200K	Pure Gaussian	0.205221	6.31673	0.0935796	-
Ex1	325K	Pseudo-Voigt	0.198958	3.89597	0.190069	0.310657
Ex2	325K	Pure Gaussian	0.0224115	4.70546	0.0388894	-
Ex3	325K	No Peak	-	-	-	-

Table 3.1.1: The estimated parameter values for the respective curves of best fit

It has been estimated that the error bar of the data points for the imaginary component of the complex dielectric function cannot exceed 0.001. Hence we use the value 0.001 as the value for our error bars.

For the Wannier exciton that gives rise to the Ex1 peak, the pseudo Voigt is the best curve of fit as compared to the Gaussian or Lorentz curves. The Gaussian character suggests inhomogeneous broadening which in turn suggests the presence of impurities or defects perturbing the local potential [14]. The Gaussian character increases as the temperature increases from 4.2K to 50K to 200K but drops at 325K, suggesting that the effect of the perturbation increases with increasing temperature in general.

We also note that although the general shape of the pseudo-Voigt curve of best fit mimics that of the data points, we note that the pseudo Voigt curve fits are not within most of the error bars for any of the temperatures. This could most likely be attributed to the slight asymmetry of the experimental data points giving rise to the Ex1 peaks.



The graphs below show the pseudo-Voigt curve of best fit together with the experimental data points and their corresponding error bars for temperature 4.2K and 200K as an example.

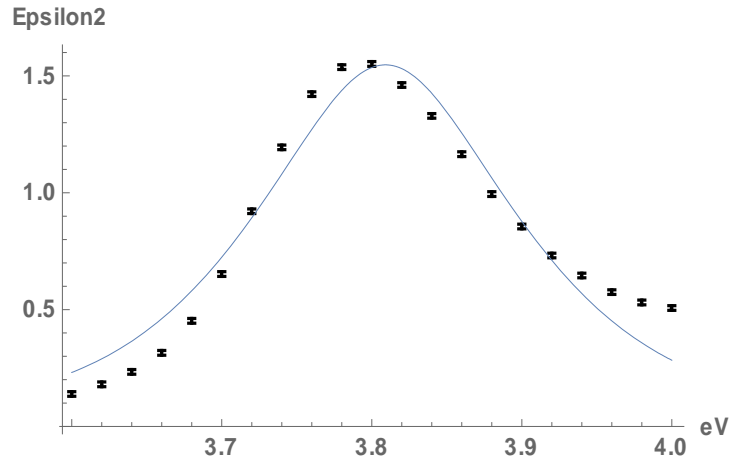


Fig 3.1.1: The data plot for Ex1 with the pseudo Voigt curve of best fit at 4.2K

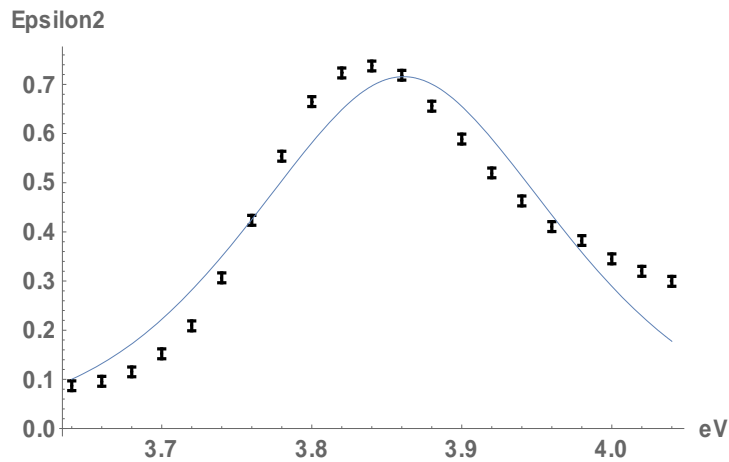


Fig 3.1.2: The data plot for Ex1 with the pseudo Voigt curve of best fit at 200K

For the resonant exciton which gives rise to the Ex2 peak in STO, the Gaussian is the best curve of fit as compared to the Voigt or Lorentz curves. The pure Gaussian nature could be due to Gaussian broadening occurring to a large extent such that the Lorentz contribution to the pseudo Voigt profile is outweighed, regardless of the temperature. It could hint that the resonant exciton responsible for Ex2 has its electronic component in a region where there is much more perturbation to the local potential due to defects or impurities as compared to the Wannier exciton responsible for Ex1.

We also note that the general shape of the Gaussian curve of best fit mimics that of the data points and is also within most of the error bars for any of the temperatures, suggesting that the Gaussian is indeed a good fit for the data points of the Ex2 peak.

The graphs below compare the fitted Gaussian curve and the fitted Lorentz curve with the data points and their corresponding error bars for temperature 4.2K as an example. The Gaussian curve fits better than the Lorentz curve.

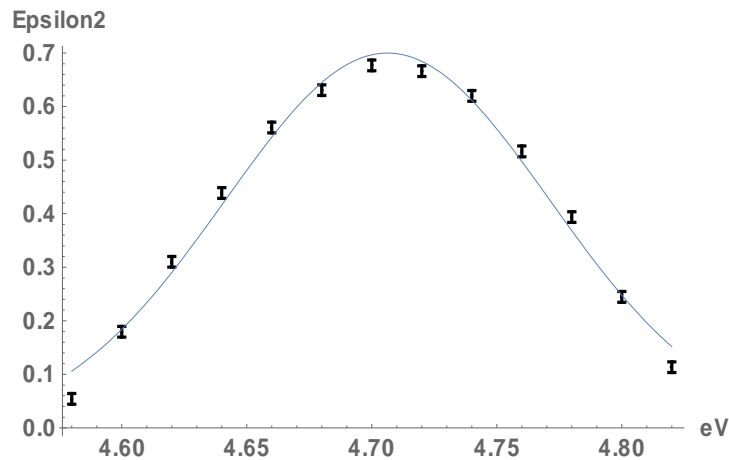


Fig 3.1.3: The data plot for Ex2 with the Gaussian curve of best fit at 4.2K

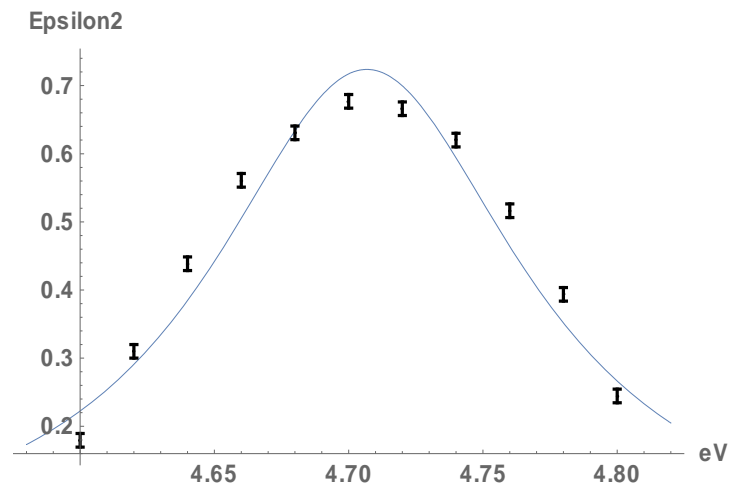


Fig 3.1.4: The data plot for Ex2 with the Lorentz curve of fit at 4.2K

Similarly, for temperature 200K as an example, the Gaussian curve fits better than the Lorentz curve. The graphs below compare the fitted Gaussian curve and the fitted Lorentz curve with the data points and their corresponding error bars for temperature 200K as an example.

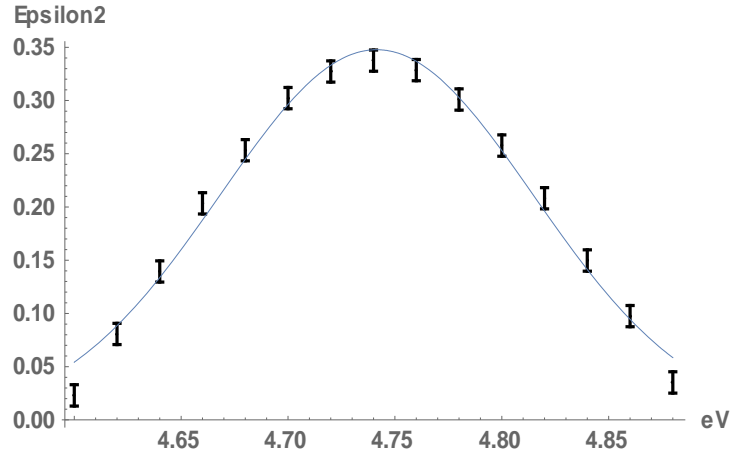


Fig 3.1.5: The data plot for Ex2 with the Gaussian curve of best fit at 200K

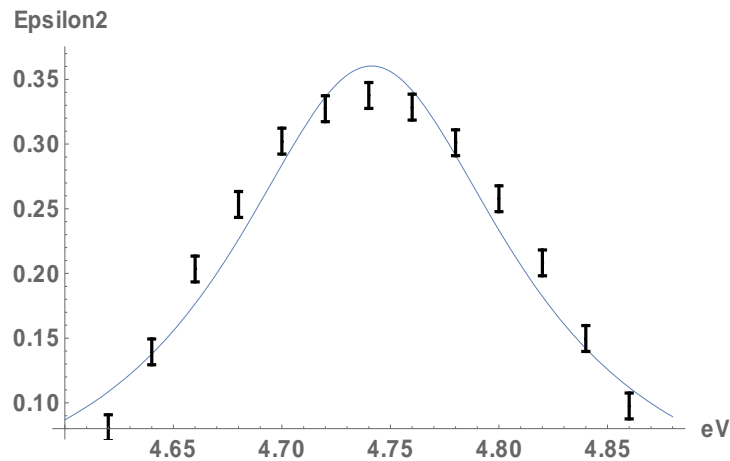


Fig 3.1.6: The data plot for Ex2 with the Lorentz curve of fit at 200K

For the resonant exciton which gives rise to the Ex3 peak in STO, the Gaussian is also the best curve of fit as compared to the Voigt or Lorentz curves. Like the resonant exciton responsible for the Ex2 peak, we can infer that the resonant exciton responsible for the Ex3 peak has its electron in a region where there is much more perturbation to the local potential due to defects or impurities as compared to the Wannier exciton responsible for Ex1.

However, the experimental data points that give rise to the Ex3 peak tend to fluctuate more than those giving rise to the Ex1 and Ex2 peaks. Hence, although the general shape of the Gaussian

curve of best fit mimics that of the data points, it is not within a majority of the error bars for any of the temperatures. In addition, there is no well defined peak for Ex3 at temperature 325K possibly due to the small difference in values of the imaginary component of the complex dielectric function experimental data points between the temperatures 325K and 350K resulting in a roughly general uniform temperature difference data.

The graphs below compare the fitted Gaussian curve and the fitted Lorentz curve with the data points and their corresponding error bars for temperature 4.2K as an example. The Gaussian curve fits better than the Lorentz curve.

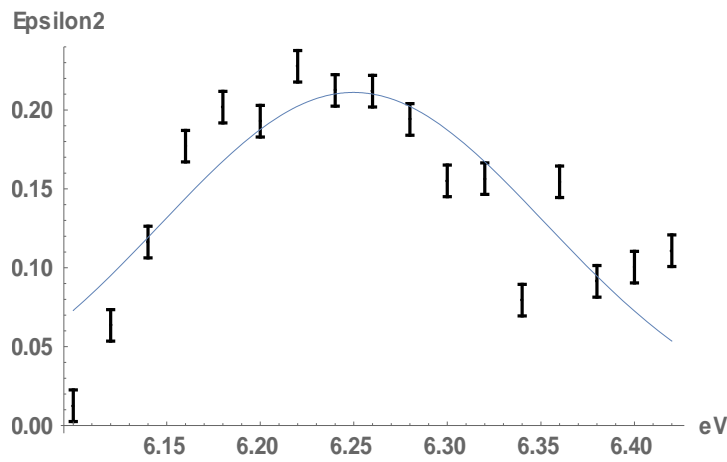


Fig 3.1.7: The data plot for Ex3 with the Gaussian curve of best fit at 4.2K

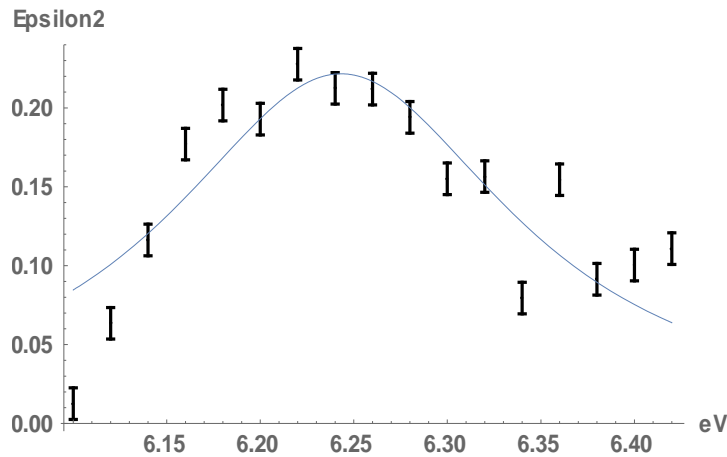


Fig 3.1.8: The data plot for Ex3 with the Lorentz curve of fit at 4.2K

Similarly, for temperature 200K as an example, the Gaussian curve fits better than the Lorentz curve. The graphs below compare the fitted Gaussian curve and the fitted Lorentz curve with the data points and their corresponding error bars for temperature 200K as an example.

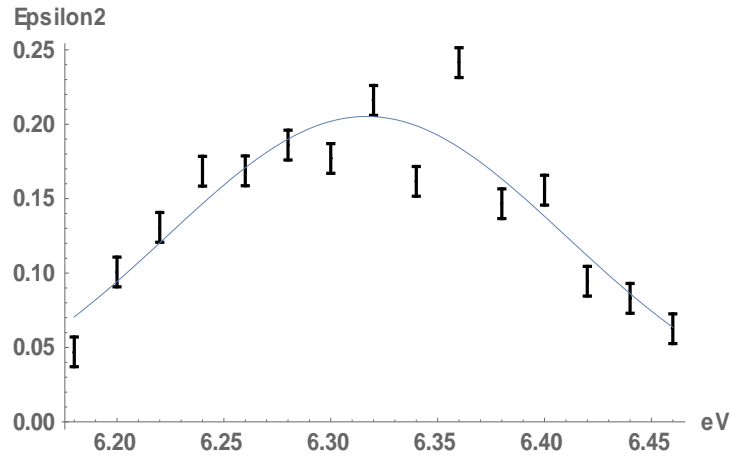


Fig 3.1.9: The data plot for Ex3 with the Gaussian curve of best fit at 200K

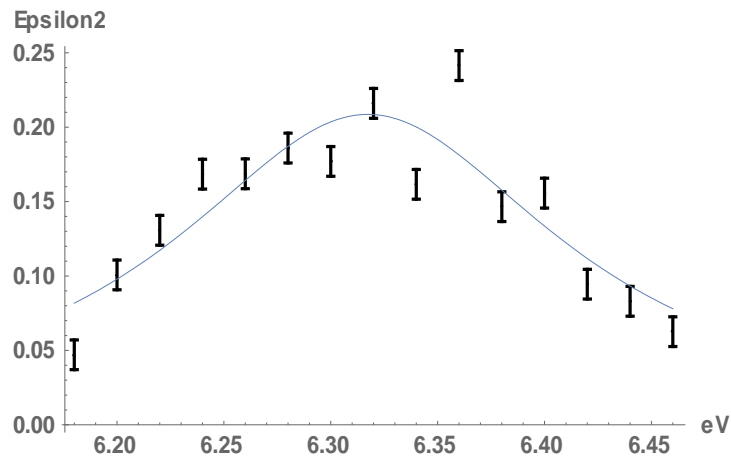


Fig 3.1.10: The data plot for Ex3 with the Lorentz curve of fit at 200K

### 3.2 The Kramers-Kronig transformation results

The following graphs show the resulting temperature difference of the real component of the complex dielectric function curves by applying the Kramers-Kronig transformation to the curves of best fit to the temperature difference of the complex component data points for the Ex1 peak compared to the experimental data points of the temperature difference of the real component of the complex dielectric function for the Ex1 peak.

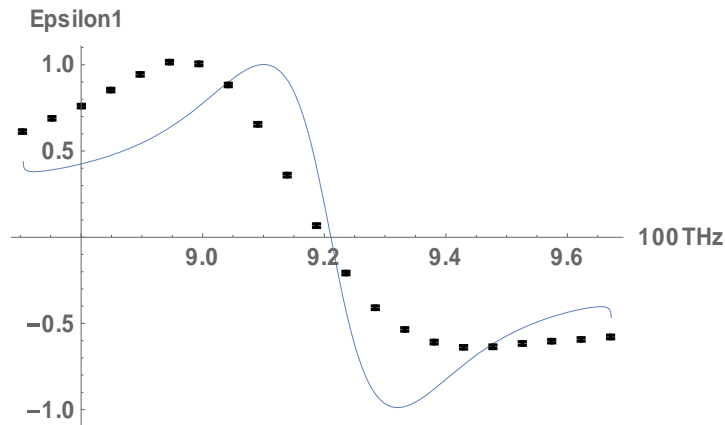


Fig 3.2.1: The data plot compared against the curve obtained via Kramers-Kronig transformation at temperature 4.2K

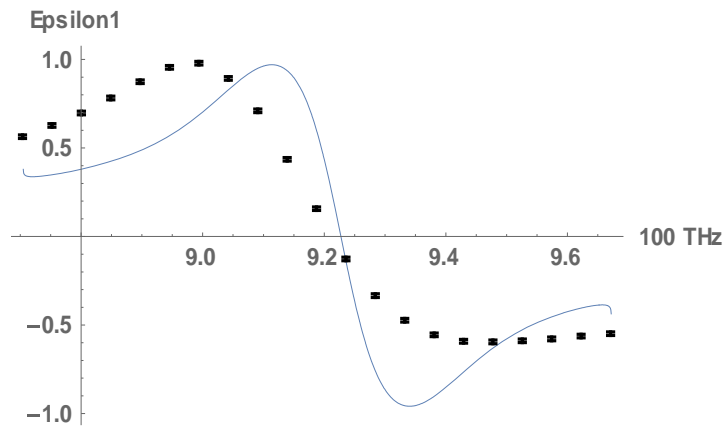


Fig 3.2.2: The data plot compared against the curve obtained via Kramers-Kronig transformation at temperature 50K

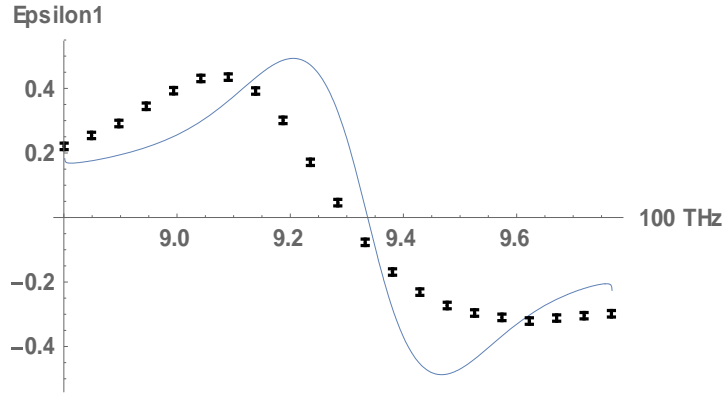


Fig 3.2.3: The data plot compared against the curve obtained via Kramers-Kronig transformation at temperature 200K

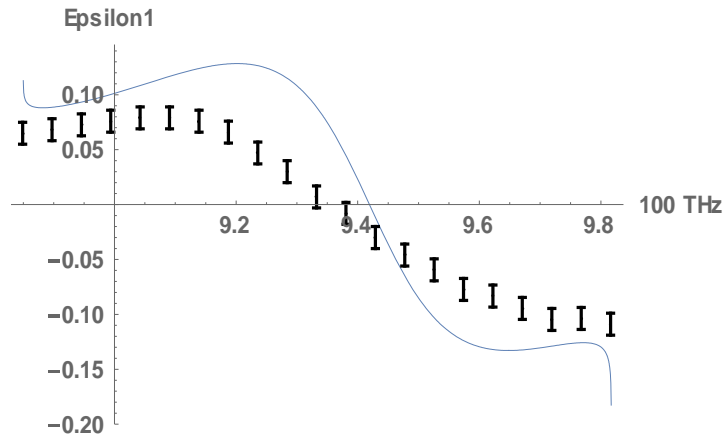


Fig 3.2.4: The data plot compared against the curve obtained via Kramers-Kronig transformation at temperature 325K

It has been estimated that the error bar of the data points for the real component of the complex dielectric function cannot exceed 0.001. Hence we use the value 0.001 as the value for our error bars.

We observe that the curves do not fit within the error bars. This is to be expected for the Kramers-Kronig transformed curve of best fit for the Ex1 peak as the Ex1 peak corresponds to a Wannier exciton. A Wannier exciton is formed through the interband transition of an electron from the valence band to conduction band and this violates the assumption of no interband transitions. However, the general shape of the Kramers-Kronig transformed curve of best fit still follows the general shape of the experimental data points for the real component of the complex dielectric function.

The following graphs show the resulting temperature difference of the real component of the complex dielectric function curves by applying the Kramers-Kronig transformation to the curves of best fit to the temperature difference of the complex component data points for the Ex2 peak compared to the experimental data points of the temperature difference of the real component of the complex dielectric function for the Ex2 peak.

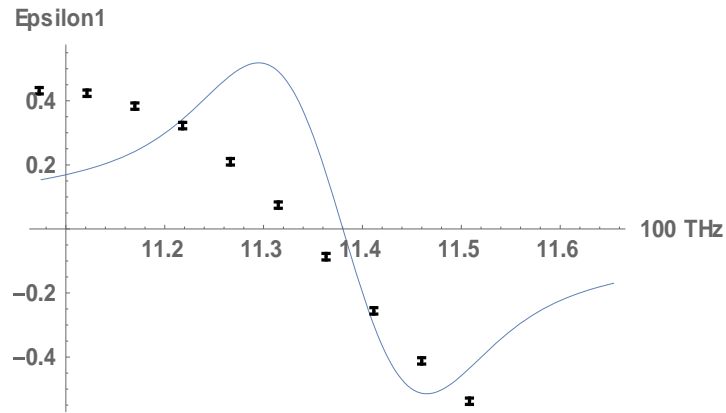


Fig 3.2.5: The data plot compared against the curve obtained via Kramers-Kronig transformation at temperature 4.2K

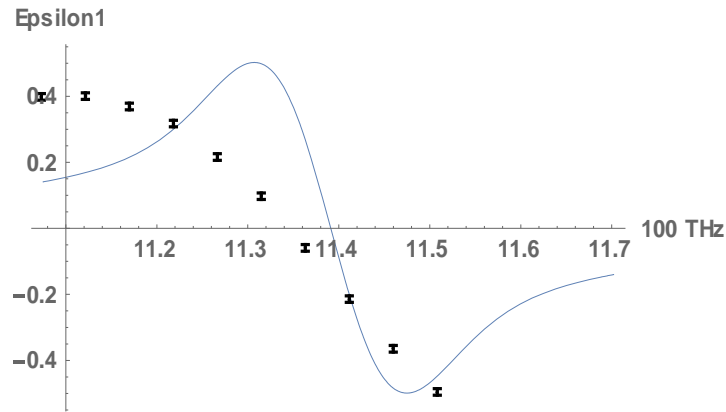


Fig 3.2.6: The data plot compared against the curve obtained via Kramers-Kronig transformation at temperature 50K



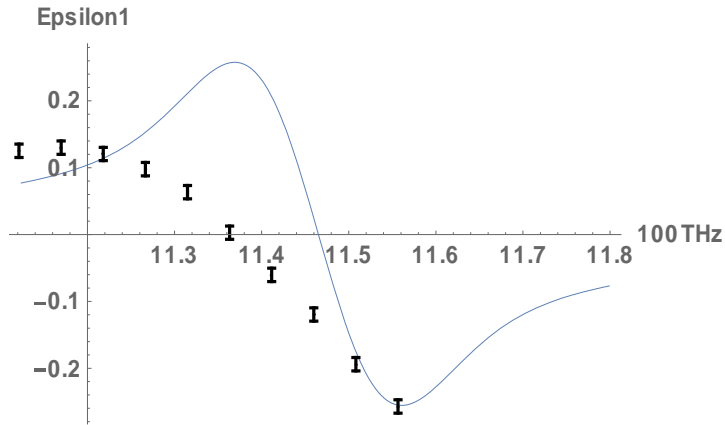


Fig 3.2.7: The data plot compared against the curve obtained via Kramers-Kronig transformation at temperature 200K

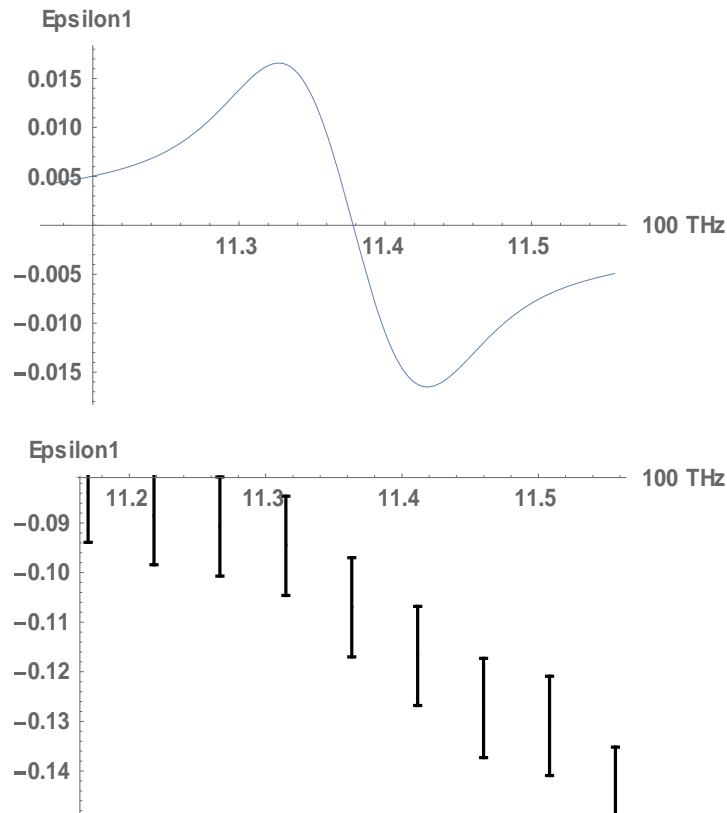


Fig 3.2.8: The data plot compared against the curve obtained via Kramers-Kronig transformation at temperature 325K

We observe that not only do the curves not fit within the error bars, the general shape of the Kramers-Kronig transformed curve of best fit fails to follow the general shape of the experimental data points for the real component of the complex dielectric function. This implies

that the assumption interband transitions do not play a role in the formation of the Ex2 resonant exciton is not valid.

The following graphs show the resulting temperature difference of the real component of the complex dielectric function curves by applying the Kramers-Kronig transformation to the curves of best fit to the temperature difference of the complex component data points for the Ex3 peak compared to the experimental data points of the temperature difference of the real component of the complex dielectric function for the Ex3 peak.

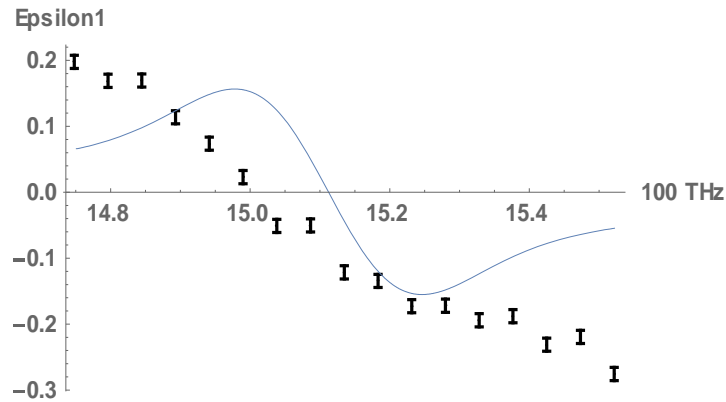


Fig 3.2.9: The data plot compared against the curve obtained via Kramers-Kronig transformation at temperature 4.2K

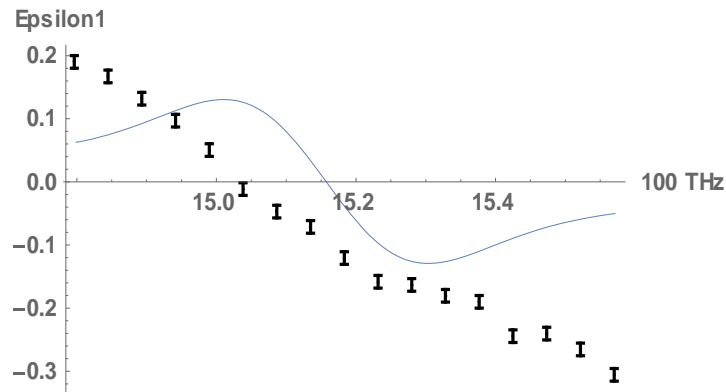


Fig 3.2.10: The data plot compared against the curve obtained via Kramers-Kronig transformation at temperature 50K

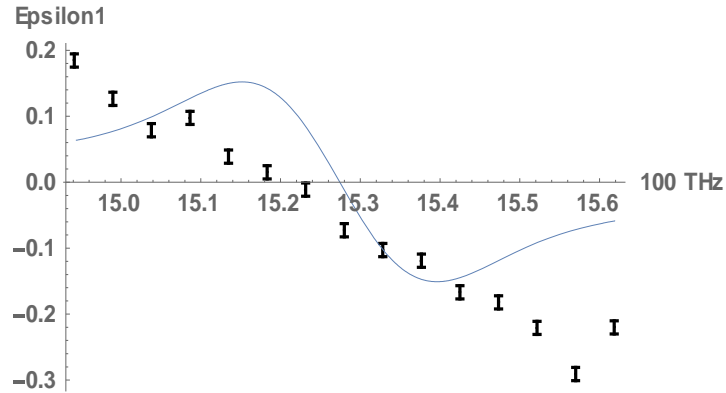


Fig 3.2.11: The data plot compared against the curve obtained via Kramers-Kronig transformation at temperature 325K

Similarly, we observe that not only do the curves not fit within the error bars, the general shape of the Kramers-Kronig transformed curve of best fit fails to follow the general shape of the experimental data points for the real component of the complex dielectric function. This implies that the assumption interband transitions do not play a role in the formation of the Ex3 resonant exciton is not valid.

A plausible reason for the general lineshape of the Kramers-Kronig transformations of the best fit curves for the resonant excitonic peaks deviate more than that of the Kramers-Kronig transformations of the best fit curves for the Wannier excitonic peaks is that the interband transitions involved in the formation of the resonant exciton span across a few different pairs of higher energy band types, as compared to the interband transitions involved in the formation of the Wannier exciton that involves only the valence and conduction band.

## **Chapter 4: Conclusion & Future Work**

### **4.1 Conclusion**

The Ex1, Ex2 and Ex3 excitonic peaks of the temperature difference of the imaginary component of the complex dielectric function were curve fitted with well known bell-shaped profiles based on the least mean square error criterion. All the curve-fitted peaks displayed a Gaussian character which implies the presence of impurities or defects in the STO sample leading to inhomogeneous broadening, with the resonant excitons experiencing greater perturbation than the Wannier excitons.

The Kramers-Kronig transformations of the best fit curves of the peaks do not fit within error bars of the data points of the temperature difference of the real component of the complex dielectric function. This implies that like the Ex1 Wannier exciton, interband transitions exist in the formation of the Ex2 and Ex3 resonant excitons. In addition the general lineshape of the Kramers-Kronig transformations of the best fit curves for the excitonic peaks deviate from the general lineshape of the data points of the temperature difference of the real component of the complex dielectric function for the Ex2 and Ex3 resonant excitons. While for the Ex1 Wannier exciton, the general lineshape of the Kramers-Kronig transformations of the best fit curves for the excitonic peaks mimic the general lineshape of the data points of the temperature difference of the real component of the complex dielectric function. This implies that while interband transitions between the valence and conduction bands can give rise to the Ex1 Wannier exciton, interband transitions involving several pairs of higher energy bands can give rise to the Ex2 and Ex3 resonant excitons.

## 4.2 Future work

There is a slight asymmetry in the Ex1 Wannier excitonic peak for the imaginary component of the complex dielectric function data points. Hence, an asymmetric pseudo Voigt profile which has to take into account many body effects multi-electron excitations in the sample [15] might be considered in future curve fitting purposes.

As the Gaussian character in all the curve fittings seem to suggest the presence of impurities or defects in the sample being used, future experiments may be carried out on STO samples with known levels of doping to check if indeed the level of Gaussian character in the new curve fittings increase with the level of doping.

The data points towards higher photon energies also tend to fluctuate more making it more difficult to do curve fitting. Future spectroscopic ellipsometry experiments could consider taking a few repeated runs and taking the average of the readings corresponding to each reading of photon energy for photon energies that are within the neighborhood of the Ex3 peak.

Finally, we should seek the higher energy bands responsible for the interband transitions that are responsible for the formation of the Ex2 and Ex3 resonant excitons in STO in future research.

## References

- [1] Hewitt, Paul G, 2006, *Conceptual Physics*, San Francisco: Pearson Addison Wesley.
- [2] Halliday, D., Resnick, R., and Walker, J., 2008, *Fundamentals of physics* (8th ed.), Hoboken, NJ: Wiley.
- [3] Huray, Paul G, 2010, *Maxwell's Equations*, Wiley-Blackwell.
- [4] Mannan Ali, 1999, Growth and study of magnetostrictive FeSiBC thin films, for device applications
- [5] Griffiths, 2014, *Introduction to Electrodynamics* 4<sup>th</sup> edition-Electromagnetic Waves, Pearson.
- [6] Martin Pope and Charles E Swenberg, 1999, *Electronic Processes in Organic Crystals and Polymers* 2<sup>nd</sup> edition, Oxford University Press
- [7] Z. Yong, P.E. Trevisanutto, L. Chiodo, I. Santoso, A.R. Barman, T.C. Asmara, S. Dhar, A. Kotlov, A. Terentjevs, F. Della Sala, V. Olevano, M. Rubhausen, T. Venkatesan and A. Rusydi, *Phy. Rev. B* 93, 205118 (2016)
- [8] Fujiwara, 2007, *Spectroscopic Ellipsometry: Principles and Applications*, John Wiley & Sons, Ltd
- [9] T. Leisegang, H. Stöcker, A. A. Levin, T. Weißbach, M. Zschornak, E. Gutmann, K. Rickers, S. Gemming, and D. C. Meyer, *Phy. Rev. Lett* 102, 087601 (2008)
- [10] Prócel, L. M., Tipán, F., & Stashans, A. (2003). Mott–Wannier excitons in the tetragonal BaTiO<sub>3</sub> lattice. *International Journal of Quantum Chemistry*, 91(4), 586590. doi:10.1002/qua.10471
- [11] F.M.F. De Groot, M. Grioni, J.C. Fuggle, J. Ghijsen, G.A. Sawatzky and H. Petersen, *Phys. Rev. B* 40 (1989), pp. 5715–5723.
- [12] P.K. Gogoi, L. Sponza, D. Schmidt, T.C. Asmara, C. Diao, J.C.W. Lim, S.M. Poh, S. Kimura, P.E. Trevisanutto, V.Olevano and A. Rusydi, *Phy. Rev. B* 92, 035119 (2015)
- [13] Bales, B. L., Peric, M., & LamyFreund, M. T. (1998). Contributions to the gaussian line broadening of the proxyl spin probe EPR spectrum due to magneticfield modulation and unresolved proton hyperfine structure. *Journal of Magnetic Resonance*, 132(2), 279286. doi:10.1006/jmre.1998.1414
- [14] P.K. Gogoi, Z. Hu, Q. Wang, A. Carvalho, D. Schmidt, X. Yin, Y. H. Chang, L.J. Li, C.H. Sow, A.H.C. Neto, M.B.H. Breese, A. Rusydi and A.T.S. Wee (2017). Oxygen Passivation Mediated Turnability of Trion and Excitons in MoS<sub>2</sub>.
- [15] Schmid, M., Steinrück, H., & Gottfried, J. M. (2014). A new asymmetric pseudovoigt function for more efficient fitting of XPS lines: New asymmetric pseudovoigt function for efficient XPS line fitting. *Surface and Interface Analysis*, 46(8), 505511. doi:10.1002/sia.5521